THE 4TH INTERNATIONAL TOPICAL MEETING ON
NUCLEAR THERMAL HYDRAULICS, OPERATIONS AND SAFETY
April 6-8, 1994, Taipei, Taiwan

FLOW CHARACTERISTICS OF COUNTER-CURRENT FLOW IN DEBRIS BED

Yutaka ABE and Hiromichi ADACHI
Yamagata University
Jonan, Yonezawa-shi, Yamagata-ken, 992, JAPAN
(0238)22-5181(Ext.353)

ABSTRACT

In the course of a severe accident, a damaged core would form a debris bed consisting of once-molten and fragmented fuel elements. It is necessary to evaluate the dryout heat flux for the judgment of the coolability of the debris bed during the severe accident. The dryout phenomena in the debris bed is dominated by the counter-current flow limitation (CCFL) in the debris bed. In this study, air-water counter-current flow behavior in the debris bed is experimentally investigated with glass particles simulating the debris beds. In this experiment, falling water flow rate and axial pressure distributions were experimentally measured. As the results, it is clarified that falling water flow rate becomes larger with the debris bed height and the pressure gradient in the upper region of the debris bed is different from that in the lower region of the debris bed. These results indicate that the dominant region for CCFL in the debris bed is identified near the top of the debris bed. Analytical results with annular flow model indicates that interfacial shear stress in the upper region of the debris bed is larger than that in the lower region of the debris bed.

INTRODUCTION

In the course of a severe accident, a debris bed is formed from once-molten and fragmented fuel elements as observed in the Three-Mile Island unit-2 accident[1]. The debris bed must be cooled to avoid further degradation of the core since the degraded core releases decay heat. Even if the degraded core is in water, it cannot be judged that the degraded core would be coolable, since the degraded core may be melted again if dryout occurs. It is thus necessary to evaluate the dryout heat flux for the judgment of the coolability of the debris bed during the severe accident[2]. Dryout phenomena in the debris bed is dominated by two-phase flow behavior in the debris bed. Especially, it is indicated that dryout phenomena in the debris bed is strongly affected by counter-current flow limitation (CCFL) in the debris bed[3]. Therefore, it is important to know the flow characteristics of CCFL in the debris bed.

Furthermore, if one hopes to analyze counter-current flow in the debris bed by using the same method as usual two-fluid model[4],[5], it is necessary to know the interfacial and wall friction factors. However, it is not clear whether the correlations for interfacial and wall friction factor for a pipe[6],[7],[8] can be applied to counter-current flow in the debris bed. In order to identify the characteristics of CCFL for two-fluid model calculation, it is necessary to determine the interfacial and wall shear stress simultaneously.

Dhir and Marschall[9],[10] measured flow rates and differential pressure at CCFL in debris bed with air-water two-phase flow. They clarified overall characteristics of CCFL in the debris bed and indicated that the characteristics of differential pressure is changed in the axial direction. However the experimental works were not enough to identify the detail flow characteristics. Inoue and Aritomi[11] conducted the experiment for co-current flow in a porous layer and concluded that co-current flow in the debris bed can be treated as annular flow. However it is not clear whether CCFL in debris bed can also be treated as annular flow or not.

In this study, flow characteristics of CCFL is investigated by using the debris bed simulated with glass particles and air-water two phase flow. Falling water flow rate for specified upward air flow rate and pressures at each elevation are measured by changing parameters of debris bed configuration such as particle diameter, debris bed height etc.. In the previous study[12], a model was developed by assuming annular flow so as to estimate the radial shear stress and velocity profile at CCFL in a pipe. In this study, this annular flow model is applied to estimate the wall and interfacial shear stress by using measured flow rates and pressure gradient.

EXPERIMENT

A. Test Rig and Experimental Procedure

In this study, air-water CCFL experiment was conducted with a debris bed simulated with glass particles. The schematic diagram of the test rig is shown in Fig.1. The test rig is divided into three parts: upper, middle and lower. Each part is made by an acrylic resin tube. Glass particles simulating debris particles are piled up on a support wire placed at boundary between middle and lower part of the test rig. In the case of fine glass particles smaller than the mesh size of the support wire, a layer of large particles are laid on the support wire to

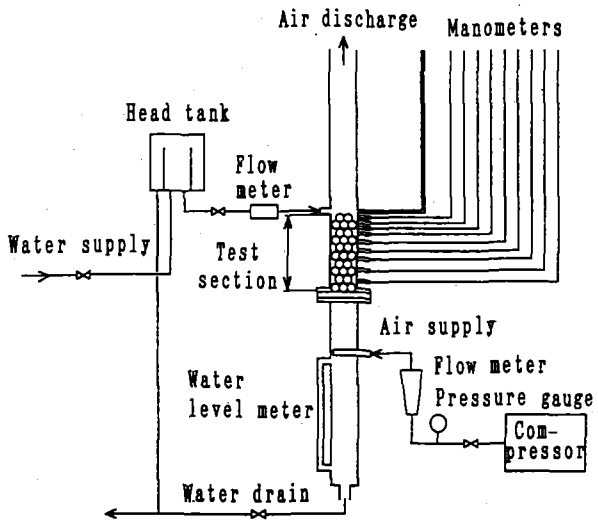

Fig.1 Schematic diagram of test rig

a layer of large particles are laid on the support wire to avoid dropping of the fine particles. Since CCFL characteristics is dominated by the layer of the smaller particles[13], a layer of the large particles at the bottom of the simulated debris bed does not affect the CCFL characteristics in the debris bed.

Air is injected from the nozzle located below the bottom of the simulated debris bed and is exhausted from the top of the test section. On the other hand, water is fed from the nozzle located just above the boundary between upper and middle parts of the test rig and is drained from the bottom of the test section.

Experimental procedures are as follows:

(1) The simulated debris bed is constructed by filling the specified glass particles up to the specified bed height on the support wire of the test section.
(2) Water drain valve is closed.
(3) Air is injected into the test section at the specified flow rate.
(4) Water is injected into the top of the simulated debris bed.
(5) Water injection rate and water drain value are controlled to keep the water level constant both in the upper part and in the bottom part of the test rig, that is, Counter-Current Flow Limitation(CCFL) is established in the test section.
(6) Water flow rate is recorded at steady state condition.
(7) Simultaneously, pressures at each axial elevation are measured by the manometers attached on the wall of the test section.
(8) Above procedures (2) through (7) are repeated for different air flow rates after draining water from the test section.

The same procedures as above (1) through (8) are conducted by changing the parameters for debris bed such as particle diameter, debris bed height, debris bed inner diameter and upper water level as shown in Table 1.

Table 1 Main parameters

Particle diameter:	**d = 3 - 19.5 mm**
Bed height:	**H_b = 20 - 200 mm**
Bed inner diameter:	**D_b = 35, 50, 70 mm**
Upper water level:	**H_{up} = 20, 100, 300 mm**
Air flow rate:	**M_g^* = 0.0 - 0.0035 m^3/s**

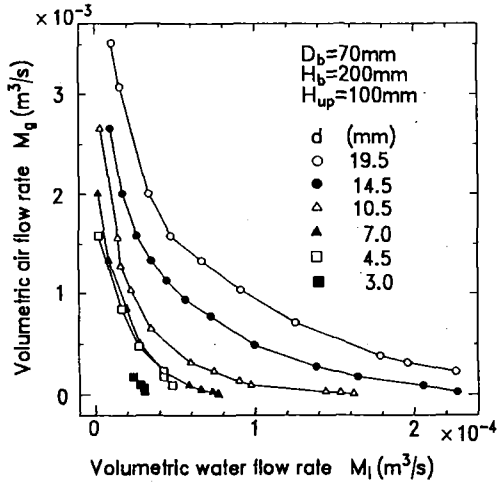

Fig.2 Measured results of volumetric flow rate

B. Experimental results

Figure 2 shows the measured falling water flow rates for specified upward air flow rates. In the experiment, the particle diameter of the debris bed is changed as a parameter. Measurement data shows the qualitative tendency that falling water flow rate decreases with upward air flow rate increasing and decreases with particle diameter.

Those measured falling water velocities and upward air velocities are rearranged with the following non-dimensional superficial velocity as shown in Fig.3,

$$J_k^* = J_k \sqrt{\frac{\rho_k}{(\rho_l - \rho_g) g L_e}} \qquad (k = l, g), \qquad (1)$$

where $$L_e = \frac{\varepsilon^3}{1-\varepsilon} \cdot \frac{d_p}{6} .$$

The non-dimensional parameters of Eq.(1) is corresponding to the Froude number. The characteristics length L_e adopted in Eq.(1) is the same as in Marschall and Dhir's experiment[9],[10]. Figure 3 indicates that the following relationship exist between the square roots of the non-dimensional air and water velocities at CCFL,

$$\sqrt{J_g^*} + \sqrt{J_l^*} = C . \qquad (2)$$

The constant C in Eq.(2) represents the magnitude of falling water velocity. Large value of the constant C means large amount of water can fall. All the data for the debris bed height H_b=200 mm are well correlated by Eq.(2) with C=0.87. This is the same result as Dhir and Marschall's experiment[9],[10].

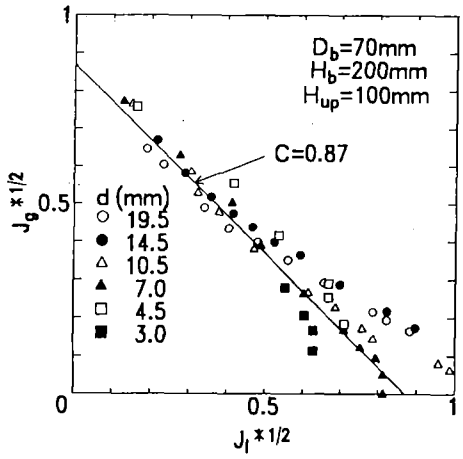

Fig.3 Relationship of non-dimensional velocity

However, the constant C changes with the debris bed height as shown in Fig.4. Figure 4 shows the relationships of non-dimensional water velocities and non-dimensional air velocities when the debris bed height is changed as a parameter. H_b' represents the bed height excluding the thickness of the bottom layer consisting larger particles. Although the constant C is almost 0.87 for higher debris bed height than 170 mm, the constant C becomes larger than 0.87 for lower debris bed than 120 mm. This result means that falling water velocity becomes large with debris bed height decreasing. That is, it is suggested that the magnitude of CCFL becomes small with debris bed height decreasing. In other words, CCFL is affected by the debris bed height.

In order to clarify this results, value of the constant C is shown in Fig.5 as a function of the debris bed height. The constant C nonlinearly increases with the bed height decreasing lower than 70 mm, although the constant C can be considered almost constant for higher debris bed height than 70 mm.

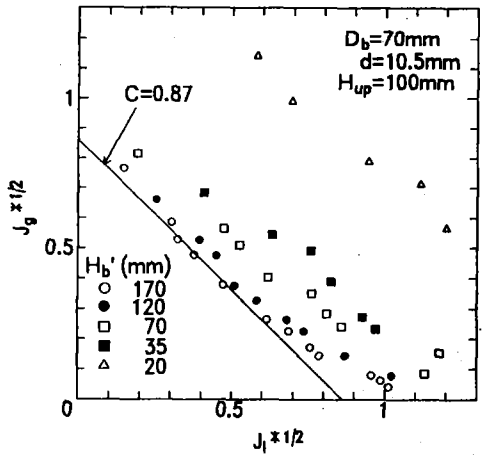

Fig.4 Effect of Debris bed height on falling water velocity

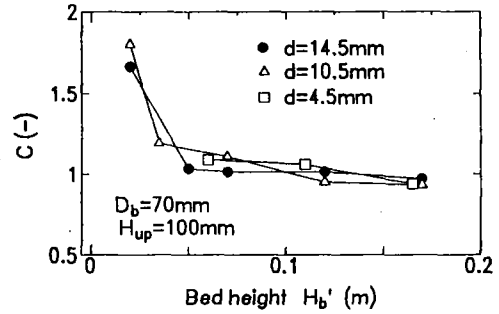

Fig.5 Effect of Debris bed height on constant C

Figure 6 shows the measurement results of pressure distribution in the axial direction. In order to compare with CCFL condition, Fig.6 includes measurement result of the pressure distributions for static water condition and single-phase down-flow condition. The measurement results of the pressure for static water is changed in the axial direction only by the static water head. In the case of single-phase down-flow, the inclination of the pressure distribution decreases with water flow rate compared with static water condition. In the cases of static water condition and single-phase down-flow conditions, the pressure linearly increases with measurement height decreasing. On the contrary, in the CCFL condition, the pressure does not change with the height in the lower region of the debris bed, although the pressure increases almost linearly with the height in the upper region of the debris bed.

The pressure gradient in the axial direction changes between the upper region and the lower region of the debris bed as shown in Fig.6. Two lines are determined for each region so as to minimize the mean square of deviation between the lines and the data, and the cross point of the two lines is determined as shown in the left graph of Fig.7. On the other hand, the measurement result of the pressure includes some oscillation. The magnitude of the oscillation is identified by the deviation between the maximum value and minimum value of the oscillation of the pressure measurement. The middle of

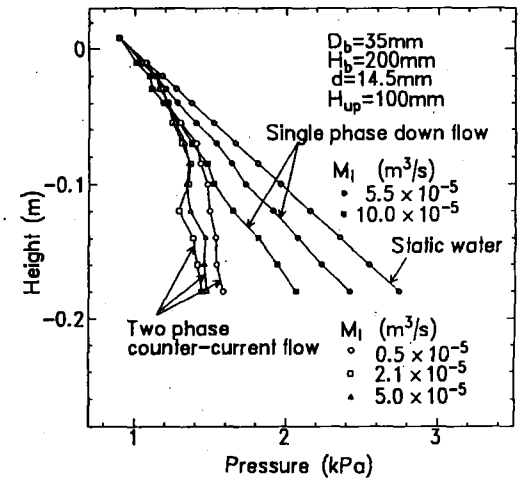

Fig.6 Measured results of axial pressure distribution

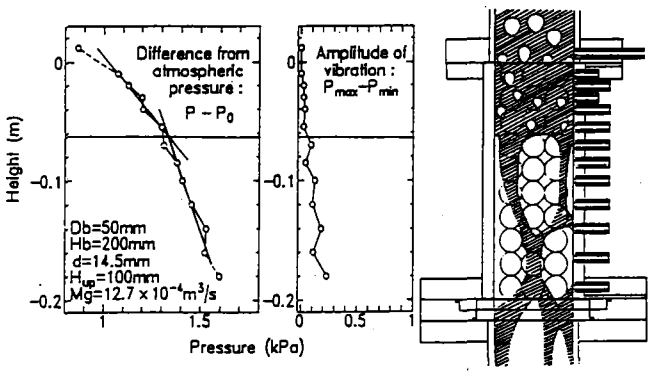

Fig.7 Comparison of Pressure distribution, amplitude of pressure fluctuation and visual observation

Fig.7 shows the distribution of the magnitude of the oscillation in the axial direction. The magnitude is smaller in the upper region of the debris bed and is larger in the lower region of the debris bed. Furthermore, visual observation reveals that gas and water are well mixed and the surfaces of the particles are always wetted in the upper region, on the other hand, the amount of water falling in the lower region is small and the water flow falling on the surface of the particles are always changing its flow path as illustrated in the right side of Fig.7. The height that the pressure gradient changes and the height that the magnitude of the pressure oscillation changes are almost agreed with the boundary of the two flow patterns. They are all at a few 10 cm below top of the debris bed.

From the experimental evidences as shown in Figs.4 and 7, it can be judged that the dominant region of CCFL is the region a few 10 cm below the top of the debris bed. That is, the reason why falling water velocity increases with the debris bed height decreasing is judged that the magnitude of the CCFL is diminished in thinner debris bed. The critical height for the CCFL is determined by two method. Figure 8 shows the measurement results of these critical heights by the two method. Fig.8(a) shows the critical height judged from the height of pressure gradient changing as shown in left graph of Fig.7. Fig.8(b) shows the critical height judged from the height of the pressure oscillation changing as shown in middle graph of Fig.7. The critical heights determined by the two methods are all concentrated in the upper region a few 10 cm below top of the debris bed.

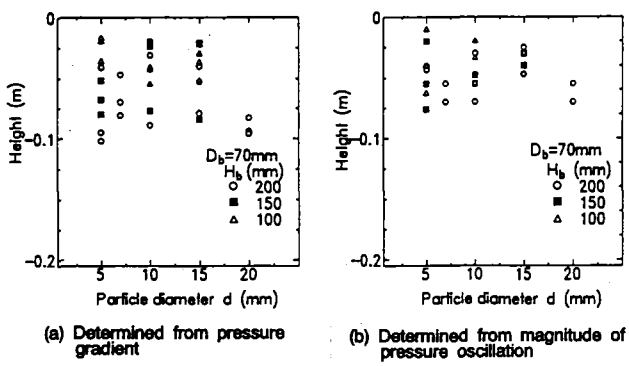

Fig.8 Dominant region for CCFL in debris bed

Therefore, it is the evident that the dominant region for CCFL in the debris bed is the upper region a few 10 cm below top of the debris bed.

ANALYSIS

A. Analytical Model

1. Basic Concept of Analytical Model

Experimental results indicates that flow characteristics at CCFL in debris bed is different between the upper region and lower region. It is important to know what is the main reason to divide the flow characteristics into two regions. A model to estimate the flow characteristics of CCFL in a pipe had already developed[12]. In this study, this model is applied to the upper region and the lower region of the debris bed so as to clarify the difference of the flow characteristics between the lower and the upper regions of the debris bed.

The basic concept of the analytical model in this study is shown in Fig.9. Observations in the experiment are shown in Fig.9(a). Gas is flowing upward and water is falling in a very complex flow geometry. Considering the fact that the gas velocity is lower than the critical velocity for channeling and higher than the value in the diffusion dominant region, it is possible to consider that a winding flow channel excluding flow branches is established as shown in Fig.9(b). As an analytical model, a hypothetical flow channel corresponding to an actual flow channel as shown in Fig.9(b) is assumed as shown in Fig.9(c). In the present study, it is assumed that counter-current annular flow is established in this hypothetical flow channel whose hydraulic diameter is calculated by

$$D_h = \frac{2}{3}\frac{\varepsilon}{(1-\varepsilon)} d_p \,. \qquad (3)$$

2. Basic Equations

The instantaneous variables are irregularly oscillating functions in two-phase flow. It is difficult to trace such microscopic behavior. In the present study, time-averaged variables are adopted and it is assumed that the change of flow variables in the axial and azimuthal directions are small compared with that in the radial direction except

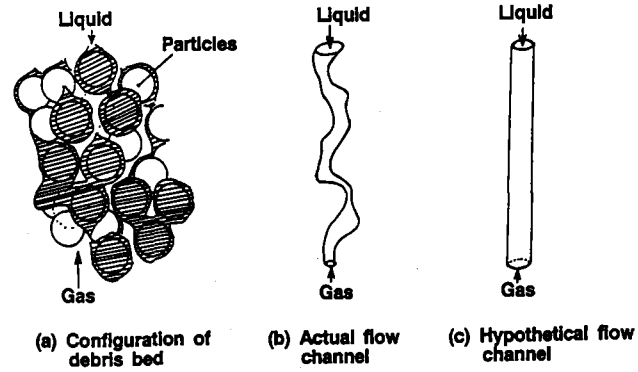

Fig.9 Basic concept of analytical model

axial change in pressure. If the flow is assumed annular, gas is flowing upward in central region of a hypothetical channel and water falls on wall of a hypothetical channel. The following momentum equations are obtained,

$$\frac{dP}{dz} + \rho_g g - \frac{2}{r}\tau = 0 \quad (\textit{for gas core}) , \tag{4}$$

$$\frac{dP}{dz} + \rho_l g - 2\frac{r\tau - r_i\tau_i}{r^2 - r_i^2} = 0 \quad (\textit{for liquid film}) . \tag{5}$$

By assuming boundary conditions at the gas-liquid interface and the wall, the following equations are also obtained,

$$\frac{dP}{dz} + \rho_g g - \frac{2}{r_i}\tau_i = 0 \quad (\textit{at interface}) , \tag{6}$$

$$\frac{dP}{dz} + \rho_l g - 2\frac{r_w\tau_w - r_i\tau_i}{r_w^2 - r_i^2} = 0 \quad (\textit{at wall}) . \tag{7}$$

By eliminating (dP/dz) from Eqs.(4) and (5) with Eq.(6), Eqs.(4) and(5) give rise to the following relationships between radial location and shear stress,

$$\tau(r) = \tau_i \frac{r}{r_i} \quad (\textit{for gas core}) , \tag{8}$$

$$\tau(r) = \tau_i \frac{r}{r_i} + \frac{2}{r}\left(1 - \frac{r_i^2}{r^2}\right)(\rho_l - \rho_g)g \quad (\textit{for liquid film}) . \tag{9}$$

Space derivatives of velocity as functions of radius r are obtained by combining Eqs.(8) and (9) with following Newton's law of viscosity,

$$\tau = \rho(\nu + \epsilon)\frac{du}{dr} . \tag{10}$$

The velocity profile in radial direction can be determined by integrating the derivatives obtained from Eqs.(8), (9) and (10) under the following boundary conditions:

(1) Velocity is continuous at the interface,
(2) Velocity is zero at the wall,
(3) The velocity gradient is zero at the center.

Once the velocity distribution u(r) is estimated, superficial velocities for each phase J_l and J_g are calculated by integrating the velocity distribution with respect to radius r. A schematic diagram of the present annular flow model described above is illustrated in Fig.10.

The relationships of Eqs.(4) and (5), and the relationships obtained from Eqs.(6) and (7) are independent of each other. Therefore, the number of the independent equations is now four. On the other hand, the number of the unknown variables is seven as follows,

(1) gas phase velocity, J_g
(2) liquid phase velocity, J_l
(3) pressure gradient, (dP/dz)
(4) void fraction, α

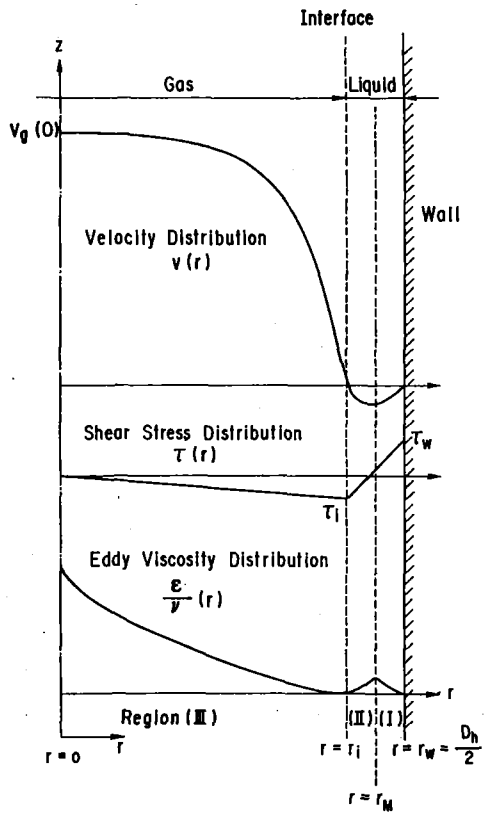

Fig.10 Description of annular flow model

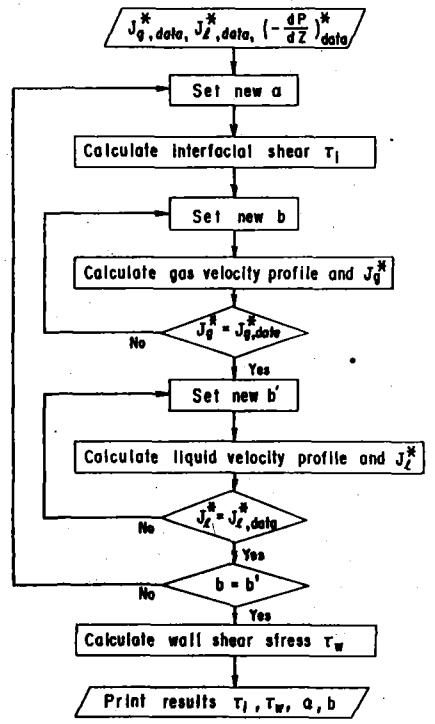

Fig.11 Solution procedure for interfacial and wall shear stress with annular flow model

(5) eddy viscosity, ε
(6) interfacial shear stress, τ_i
and (7) wall shear stress. τ_w.

If three of these seven unknowns are given, the other four variables can be determined with the above four relationships. Since the velocities for each phase and the pressure gradient are measured in the present experiment, the other variables can be calculated by using the solution procedure shown in Fig.11. This approach gives a method to evaluate the wall and interfacial shear stresses and the void fraction at CCFL in the debris bed with the measured gas and liquid velocities and pressure gradient. In the above solution procedure, void fraction is related to the location of the interface based on geometrical consideration as

$$r_i = \frac{D_h}{2}\sqrt{\alpha} \quad . \qquad (11)$$

3. Turbulent Model

If the flow is laminar, the eddy viscosity in Eq.(10) can be set to zero. However, the liquid phase seems to be very agitated in counter-current flow in debris bed. It is impossible to assume the eddy viscosity in Eq.(10) zero for any condition. In the present study, the eddy viscosity is expressed in a similar form to Sleicher's equation[14] as

$$\frac{\varepsilon}{\nu_l} = b^2 y^{+2} \quad . \qquad (12)$$

In the present study, the disturbance is assumed to be generated at the wall and gas-liquid interface. Therefore, the dependent variable y in Eq.(12) is defined as the distance from the wall in region (I) or from the interface in regions (II) and (III) as shown in Fig.10. Although the eddy viscosity for co-current flow in a pipe was measured by Sekoguchi[15], the eddy viscosity at CCFL in the debris bed is not clear at present. Therefore, the constant b in Eq. (12) is taken as an unknown constant and is determined by iterative calculations to match the measured data as shown in Fig.11. It is thought that the effect of the agitated interface on the velocity profile and shear stress profile is taken into account by constant b, because the velocity distribution and shear stress distribution in the radial direction is affected by the eddy viscosity expressed in Eqs.(10) and (12) including b. Since there is still uncertainty on the treatment of the eddy viscosity in Eqs.(10) and (12), more experimental study on the eddy viscosity in CCF is expected.

B. Analytical Results

Figure 12 shows the measurement results of the pressure gradients determined for the upper and the lower region in the debris bed. Although the experimental data scatter in wide range, it is very clear that the measured pressure gradient in the upper region of the debris bed is larger than that in the lower region of the debris bed. Figure 12 also includes the measured data by Dhir et al.[9][10]. Dhir et al. determined the pressure gradient as the mean value for whole length of the debris bed. As shown in Fig.12, the Dhir's data are between the present data of the upper region of the debris bed and that of the lower region of the debris bed.

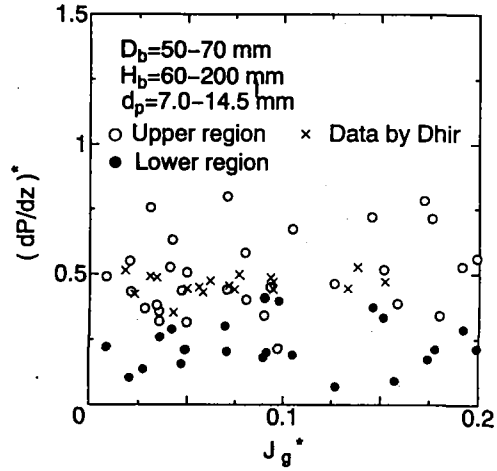

Fig.12 Measurement results of pressure gradient

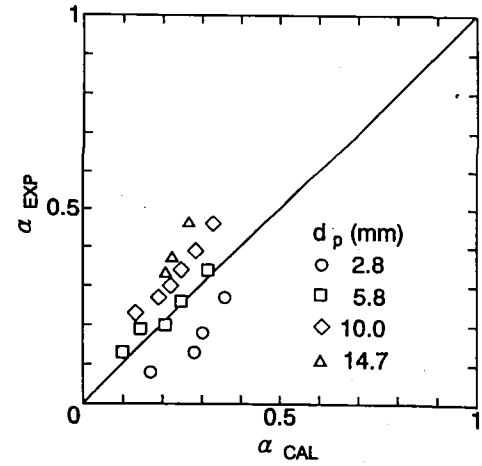

Fig.13 Comparison of void fraction between measured data and evaluated results with annular flow model

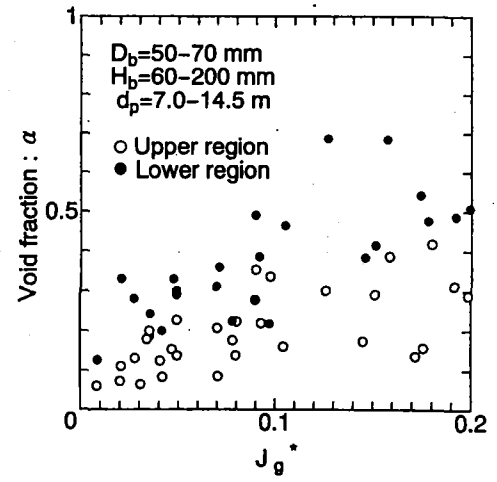

Fig.14 Void fraction evaluated with annular flow model

Dhir et al. also measured the void fraction in their CCFL experiment. The measured data for the void fraction are compared with the calculated results with the present model to check the validity of the present method. As shown in Fig.13, the experimental data scatter in the range lower than 0.5, although void fraction of annular flow in a pipe is higher than 0.75. Since there is not enough information on the flow pattern of the two-phase flow in the debris bed, it is difficult to judge the actual flow pattern of CCFL in the debris bed. However, calculated results are in almost the same range as the experimental data. It can be judged that the calculated results show moderate agreement with the data. It is recommended to conduct the experiment works to obtain the more detail information on the void fraction at CCFL in the debris bed.

In order to clarify the difference of the flow characteristics between the upper region and the lower region of the debris bed, calculations are conducted for the upper region and the lower region of the debris bed separately. Figure 14 shows the calculated results of the void fractions for the upper region and the lower region of the debris bed. It is very clear that the void fraction in the upper region of the debris bed is lower than that in the lower region of the debris bed. This result is corresponding to the observation result indicating that much water is accumulated in the upper region of the debris bed.

Figure 15 shows the interfacial shear stresses and Figure 16 shows the wall shear stresses evaluated with the present model. The downward flow of water is determined by the balance of gravitational force and the interfacial and the wall friction forces in two-phase flow. It is known from Figs.15 and 16 that the shear stress acting on the liquid film at the wall is of about the same order as that at gas-liquid interface. It is very clear that the interfacial shear stress in the upper region is larger than that in the lower region of the debris bed, although difference of wall shear stress between in the upper region and the lower region can not be recognized. It can be judged from this results that CCFL in the debris bed is dominated by the large interfacial shear stress in the upper region of the debris bed.

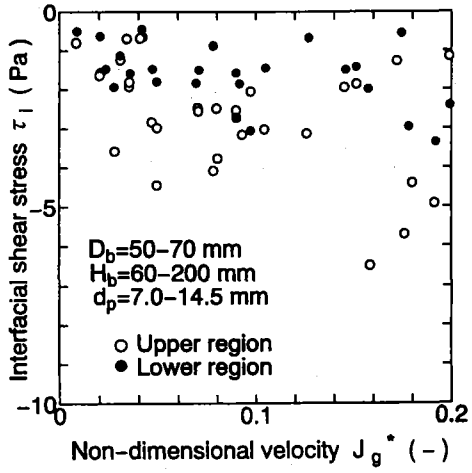

Fig.15 Interfacial shear stress evaluated with annular flow model

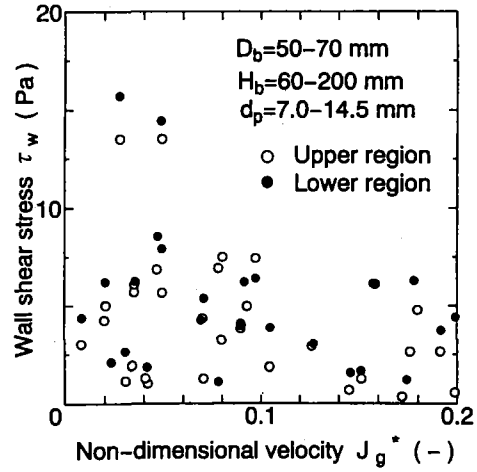

Fig.16 Wall shear stress evaluated with annular flow model

CONCLUSIONS

It is experimentally clarified that the constant C indicating the amount of the falling water velocity increases with the debris bed height decreasing.

The measured pressure gradient at CCFL in the debris bed changes at some critical height. The pressure distribution can be approximated with two lines. The pressure gradient in the upper region is larger than the pressure gradient in the lower region.

The magnitude of the pressure oscillation at CCFL in the upper region is smaller than that in the lower region.

The height that pressure gradient changes and the height that the magnitude of the pressure oscillation changes are almost agreed with the height that the flow pattern changes. They are all a few 10 mm below top of the debris bed. It can be judged that the upper is the dominant region for CCFL in the debris bed.

Annular flow model is applied to the present experimental data to estimate void fraction and wall and interfacial shear stresses for the CCFL dominant region and the lower region.

The estimated void fraction for the CCFL dominant region is smaller than the lower region. Absolute value of the estimated interfacial shear stress in the CCFL dominant region is larger than that in the lower region, although it is difficult to identify the difference of the wall shear stress between the upper CCFL dominant region and the lower region.

Acknowledgement

The authors wish to acknowledge Mr. Takehisa Murayama of Koparu Corporation and Mr. Harumitu Yokoyama of Hitachi Zosen Corporation who worked with authors to obtain the experimental data.

REFERENCES

1. Brown, G.R.,et al.: GEND-055(1986).
2. Lipinski, R.J.: Trans.Am.Nucl.Soc., 35,(1980),361.
3. Abe,Y. and Sudo,Y.: J.Nucl.Sci.Technol., 21(12), (1984),962-964.
4. Liles, D.R.,et al.: NUREG/CR-3858 LA-10157-MS, (1986).
5. Ransom, V.H.,et al.: NUREG/CR-4312 EGG-2396, (1987).
6. Wallis, G.B.: "One-dimensional two-phase flow", McGraw-Hill, (1969).
7. Bharathan, D., Wallis, G.B.: Int. J. Multiphase Flow, 9(4),(1983),349-366.
8. Ergun, S.: Chem. Eng. Prog., 48,(1952),89-94.
9. Marshall, J.S. and Dhir, V.K.:NUREG/CR-3995, (1984).
10. V.K.Dhir,"Some Aspects of Two Phase Flow Through Porous Media", Nucl. Eng. Des., 95 (1986), 275-283
11. Inoue,A., Aritomi,M., et al.: 3'd Int. Top. Mtg. Nucl. Power Plant Therm. Hydr. and Ope., Seoul Koria, (Nov.1988), A1-34-41
12. Abe, Y. et al.:Six Proc.Nucl.Therm.Hydr.1990 ANS Winter Mtg.,(1990)401-408.
13. Maruyama, Y. and Abe, Y., et al.: JAERI-M 88-157, (in Japanese) (1988)
14. Sleicher,Jr. C.A.: Trans.ASME,80 , 693-704, (1958).
15. Sekoguchi,K., et al.: J.JSME (in Japanese) 39(317), (1973),313-323

NOMENCLATURE

b: Constant (-)
d_p: Particle diameter (m)
D_h: Hydraulic diameter (m)
D^*: Non-dimensional hydraulic diameter (-)
f: Friction factor (-)
g: Acceleration due to gravity (m/s^2)
J: Superficial velocity (m/s)
J^*: Non-dimensional superficial velocity (-)
P: Pressure (N/m^2)
Re: Reynolds number (-)
r: Radius (m)
u: Local velocity (m/s)
V: Mean velocity (m/s)
y: Distance from source of disturbance (m)
y^+: Non-dimensional radius (-)
z: Axial distance (m)

Greek

α : Void fraction (-)
ε : Porosity (-)
μ : Viscosity (kg/ms)
ν : Kinematic Viscosity (m^2/s)
ρ : Density (kg/m^3)
σ : Surface tension (N/m)
τ : Shear stress (N/m^2)
δ : Film thickness (m)
δ^* : Non-dimensional film thickness (-)

Subscripts

g: Gas phase
i: Interface
l: Liquid phase
w: Wall